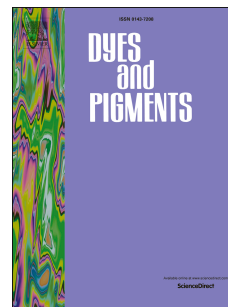


Accepted Manuscript

The design and synthesis of thiophene-based ruthenium(II) complexes as promising sensitizers for dye-sensitized solar cells

A.V. Medved'ko, V.K. Ivanov, M.A. Kiskin, A.A. Sadovnikov, E.S. Apostolova, V.A. Grinberg, V.V. Emets, A.O. Chizov, O.M. Nikitin, T.V. Magdesieva, S.A. Kozyukhin



PII: S0143-7208(17)30071-2

DOI: [10.1016/j.dyepig.2017.01.030](https://doi.org/10.1016/j.dyepig.2017.01.030)

Reference: DYPI 5729

To appear in: *Dyes and Pigments*

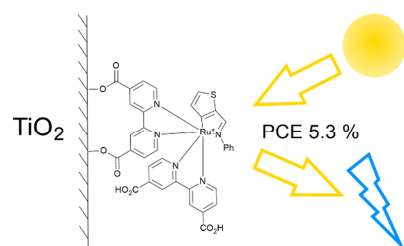
Received Date: 29 July 2016

Revised Date: 14 October 2016

Accepted Date: 12 January 2017

Please cite this article as: Medved'ko AV, Ivanov VK, Kiskin MA, Sadovnikov AA, Apostolova ES, Grinberg VA, Emets VV, Chizov AO, Nikitin OM, Magdesieva TV, Kozyukhin SA, The design and synthesis of thiophene-based ruthenium(II) complexes as promising sensitizers for dye-sensitized solar cells, *Dyes and Pigments* (2017), doi: 10.1016/j.dyepig.2017.01.030.

This is a PDF file of an unedited manuscript that has been accepted for publication. As a service to our customers we are providing this early version of the manuscript. The manuscript will undergo copyediting, typesetting, and review of the resulting proof before it is published in its final form. Please note that during the production process errors may be discovered which could affect the content, and all legal disclaimers that apply to the journal pertain.



ACCEPTED MANUSCRIPT

The design and synthesis of thiophene-based ruthenium(II) complexes as promising sensitizers for dye-sensitized solar cells



A. V. Medved'ko,^{*a,b} V. K. Ivanov,^{c,d} M. A. Kiskin,^c A. A. Sadovnikov,^c E. S. Apostolova,^e V. A. Grinberg,^f V. V. Emets,^f A. O. Chizov,^g O. M. Nikitin,^{a,h} T. V. Magdesieva^a and S. A. Kozyukhin^{c,d}

^a Department of Chemistry, Lomonosov Moscow State University, Moscow, 119991, Russia. *medved'ko@org.chem.msu.ru

^b The Photochemistry Center, RAS, Moscow, 119421, Russia.

^c Kurnakov Institute of General and Inorganic Chemistry, RAS, Moscow, 119991, Russia.

^d Department of Chemistry, National Research Tomsk State University, Tomsk, 634050, Russia.

^e Mendeleev University of Chemical Technology, Moscow, 125047, Russia

^f Frumkin Institute of Physical Chemistry and Electrochemistry, RAS, Moscow, 119071, Russia

^g Zelinsky Institute of Organic Chemistry, RAS, Moscow, 119991, Russia

^h A.N. Nesmeyanov Institute of Organoelement Compounds, RAS, Moscow, Russia

Keywords: Cyclometallation; Ruthenium(II) sensitizer; Thiophene; Electronic spectra; DFT; Dye-sensitized solar cells

Abstract

A new series of promising synthetically facile cycloruthenated thiophene-based sensitizers have been developed and fully characterized by UV-vis spectroscopy, NMR and cyclic voltammetric studies. The synthesized dyes have broad MLCT bands spanning the visible spectrum, with high extinction coefficients. The energies of the molecular orbitals for the isolated molecules of the complexes and densities of occupied states were determined. The cycloruthenated compounds contains *ortho*-metallated thiophene moiety substituted by N-(methylidene)aniline or pyridine-2-yl at the *ortho*-position. Having 4,4'-dicarboxy-2,2'-bipyridine as the linker and auxiliary ligands and anchored to nanocrystalline TiO₂ films, they achieve

efficient sensitization in the visible range and display an overall conversion efficiency of 5.3% under standard AM 1.5 sunlight.

1. Introduction

The search for sustainable sources of renewable energy is one of the greatest challenges to 21st century civilization. Among existing energy sources, a conversion of solar energy to electric power (photovoltaics, PV) is one of the most attractive technologies. According to the International Energy Agency Photovoltaic Power Systems Programme (IEA-PVPS) report, energy production of PV systems increased up to 36.9 GW in the year 2013 as compared to 29 GW in the year 2012 [1]. Traditional monocrystalline Si-based solar cells can reach 27% power conversion efficiency (PCE) [2]. The new type of multijunction cell containing Ga, As, In, N, P elements gave 43.5% PCE [3]. However, the fabrication of such solar cells requires very clean conditions (for Si-based cells) or the use of toxic elements (for SJ3-type cells). Thus, nowadays traditional photovoltaic technology faces strong competition from third generation PV (3GPV) technology, especially dye-sensitized solar cells (DSSC) and organic solar cells. PCE reached 13% for the former [4] and 12.05% for the latter [5]. PCE of all-solid-state dye-sensitized solar cells based on lead-halide organic-inorganic perovskites have quickly increased over the last six years [6], and the performance of the cells with a National Renewable Energy Laboratory (NREL)-certified reached record efficiency of 22.1%. DSSCs have a leading edge over other technologies due to their lower cost, simple fabrication methods and high power conversion efficiency. In these cells, the dye is one of the key components for high PCE.

A typical ruthenium(II) dye for DSSCs based on mesoporous titania film utilizes three types of ligands – a linker which connects Ru to the TiO₂ surface [7]; an anionic ligand modulating HOMO energy; an auxiliary ligand modulating LUMO energy [8]. Linking and anionic ligands are usually 2,2'-bipyridine-4,4'-dicarboxylic acid and two thiocyanate moieties, respectively. A lot of different auxiliary and linking lig-

ands were probed to enhance the PCE of solar cells [9]. Maximal PCE value for NCS-containing equals 11.5% [10]. The main drawback of these dyes is their low photostability and thermal stability [11]. Another type of anionic ligand is 2-phenylpyridine and its derivatives. The PCE of corresponding DSSCs reached 10.1% [12]. Attempts to replace 2-phenylpyridine with other similar ligands were also made [13–16]. One very promising ligand is *ortho*-substituted thiophene. Recently it has been shown that thiophene derivatives containing a coordinating ligand at the 2-position can be metallated to the 3-position to give cycloruthenated compounds [17,18]. The usage of corresponding complexes as sensitizers in DSSCs was considered in one report only [19]. In the present paper, the preparation of the simplest cycloruthenated compounds containing *ortho*-metallated thiophene moiety substituted by N-(methylidene)aniline or pyridine-2-yl at the *ortho*-position, with traditional 4,4'-dicarboxy-2,2'-bipyridine as the linker and auxiliary ligands is reported. To get an insight of the substituent influence on the dyes electronic properties, their electrochemical, spectral and DFT studies were carried out. To determine the solar energy conversion efficiency of new d⁶-ruthenium-based organometallic sensitizers, testing their performance in DSSCs was carried out.

2. Experimental section

2.1. Materials and instruments

All starting reagents were obtained from commercial sources. The solvents were dried prior to the use by conventional methods. Di- μ -chlorobis((η^6 -benzene)ruthenium(II) chloride) [20] and diethyl 2,2'-bipyridine-4,4'-dicarboxylate [21] were prepared as described elsewhere. ¹H and ¹³C NMR spectra were obtained on Bruker DRX-400 and AVANCE-500 spectrometers. Elemental analysis was carried out on a Eurovector EA 3000 automated analyzer. Electronic spectra were registered at room temperature on a Cary5000 UV-vis-NIR spectrometer (Agilent) equipped with DRA2500. High resolution mass spectra (HRMS) were measured on a Bruker micrOTOF II instrument using electrospray ionization (ESI) [22].

The measurements were made in a positive ion mode (interface capillary voltage – 4500 V). Mass range was from m/z 50 to m/z 3000; external or internal calibration was done with ESITuningMix, Agilent. A syringe injection was used for solutions in acetonitrile (flow rate 3 $\mu\text{L}/\text{min}$). For compounds **7** and **8**, triethylamine was added to enhance solubility. Nitrogen was applied as dry gas; interface temperature was set at 180 °C. The HRMS values are presented for the most abundant peak in the isotope cluster.

2.2. Synthesis and characterization of dyes

***N*-(thiophen-2-ylmethylidene)aniline (1)**. Synthesized as described previously [23]. Yield 72%. δH (400 MHz, CDCl_3 , 27 °C): 7.14-7.16 (dd, 1H, 4-H-anil, $^3J_{\text{H,H}} = 4.8, 3.8$ Hz), 7.20-7.25 (m, 3H, 2-H-anil, 4-H-th), 7.38-7.42 (m, 2H, 3-H-anil), 7.47-7.51 (m, 2H, 3,5-H-th), 8.56 (s, 1H, CH=N).

2-Bromothiophene. Synthesized as described previously [24]. Yield 58 %. Bp 53-56 °C (18 mmHg). δH (400 MHz, CDCl_3 , 27°C): 6.87 (dd, 1H, 4-H, $^3J_{\text{H,H}} = 5.5, 3.7$ Hz), 7.05 (dd, 1H, 3-H, $^3J_{\text{H,H}} = 1.7, 3.7$ Hz), 7.23 (dd, 1H, 5-H, $^3J_{\text{H,H}} = 5.5, 1.3$ Hz).

2-(thiophen-2-yl)pyridine (2). Synthesized as described previously [25] and purified as follows. Sticky solid obtained after washing with ammonium chloride solution was filtered off through Celite and washed with 160 ml of diethyl ether until slight coloration of the washings. Then the water phase was extracted with 30 ml of diethyl ether. Organic phases were combined and washed with 30 ml of brine. The organic phase was dried over magnesium sulfate. The solvent was removed on a rotary evaporator. The residue was dissolved in hot pentane. Upon cooling to room temperature red oil was precipitated. Pentane solution was decanted from oil. The solvent was removed on a rotary evaporator. The residue was crystallized from the mixture of pentane and petroleum ether to give yellow needles of the product. The solvent from mother liquor was removed on a rotary evaporator. The residue was purified with column chromatography on silica gel (eluent: petroleum ether: ethyl acetate 4:1). 3.76 g (83%) of yellow needles was ob-

tained. δ H (400 MHz, CDCl_3 , 27 °C): 7.09-7.15 (m, 2H, 4-H-th, 5-H-Py), 7.38 (m, 1H, 5-H-th), 7.58 (m, 1H, 3-H-th), 7.63-7.69 (m, 2H, 3,4-H-Py), 8.55-8.57 (m, 1H, 6-H-Py).

General procedure for synthesis of compounds 3 and 4. Synthesized analogously to [26] and purified by column chromatography on silica gel (eluent DCM:MeCN 10:1). The product was dissolved in a minimum volume of DCM and precipitated with petroleum ether.

Tetrakis(acetonitrile)[N-((thiophene-2-yl- κ C³)methyliden)ani-line- κ N]ruthenium(II) hexafluorophosphate (3). Orange powder. Yield 30%. Single crystals were grown by vapor diffusion of petroleum ether into benzene/methanol solution of the product. δ H (400 MHz, CD_3CN , 27 °C): 1.96 (s, 3H, CH₃), 2.12 (s, 6H, CH₃), 2.51 (s, 3H, CH₃), 7.28-7.33 (m, 3H, 2,4-H-anil), 7.41-7.45 (m, 2H, 3-H-anil,) 7.62 (d, 1H, th, $^3J_{\text{H,H}} = 4.7$ Hz), 7.83 (d, 1H, th, $^3J_{\text{H,H}} = 4.7$ Hz), 8.40 (s, 1H, CH=N).

Tetrakis(acetonitrile)[2-(thiophen-2-yl- κ C³)pyridine- κ N]ruthenium(II) hexafluorophosphate (4). Yellow powder. Yield 45%. Single crystals were grown by vapor diffusion of diethyl ether into chloroform solution of the product. δ H (400 MHz, CD_3CN , 27 °C): 1.96 (s, CH₃, 3H), 2.03 (s, 6H, CH₃), 2.51 (s, 3H, CH₃), 6.98 (m, 1H, Py), 7.43 (d, 1H, 3-H-Py, $^3J_{\text{H,H}} = 8.1$ Hz), 7.49 (d, 1H, th, $^3J_{\text{H,H}} = 4.7$ Hz), 7.56 (d, 1H, th, $^3J_{\text{H,H}} = 4.7$ Hz), 7.65 (td, 1H, Py, $^3J_{\text{H,H}} = 8.9, 1.4$ Hz), 8.73 (d, 1H, 6-H-Py, $^3J_{\text{H,H}} = 5.5$ Hz).

General procedure for synthesis of compounds 5 and 6. Synthesized analogously to [18] and purified by column chromatography on silica gel (eluent DCM:MeOH 25:1). The product was dissolved in a minimum volume of DCM and precipitated with petroleum ether.

Bis(4,4'-diethoxycarbonyl-2,2'-bipyridine- $\kappa^2\text{N,N}'$)[N-((thio-phen-2-yl- κ C³)methyliden)aniline- κ N]ruthenium(II) hexafluorophosphate (5). Red solid. Yield 77%. δ H (400 MHz, CDCl_3 , 27 °C): 1.39-1.49 (m, 12H, CH₃), 4.41-4.53 (m, 8H, CH₂), 6.37 (m, 3H, 4-H-th, 2,6-H-anil), 6.90-6.93 (m, 2H, 3,5-H-anil), 6.94-6.97 (m, 1H, 4-H-anil), 7.64 (d, 1H, 5-H-th, $^3J_{\text{H,H}} = 4.6$ Hz), 7.80 (dd, 1H, 5-H-Py, $^3J_{\text{H,H}} = 6.0, 1.4$ Hz), 7.86-7.89 (m, 3H, 5,6-H-Py), 7.95 (d, 1H, 6-H-Py, $^3J_{\text{H,H}} = 6.0$ Hz), 8.00-8.03 (m, 2H, 5,6-H-Py),

8.47 (s, 1H, 3-H-Py), 8.54 (s, 1H, 3-H-Py), 8.59 (s, 1H, CH=N), 8.74 (d, 1H, 6-H-Py), 8.80 (s, 1H, 3-H-Py), 8.84 (s, 1H, 3-H-Py). δC (100 MHz, CDCl_3 , 27 °C): 14.07 (CH₃); 14.15 (CH₃); 14.18 (CH₃); 62.57 (CH₂); 62.62 (CH₂); 62.71 (CH₂); 121.39 (2,6-CH-anil); 121.76 (3-CH-Py); 121.82 (3-CH-Py); 121.22 (3-CH-Py); 121.29 (3-CH-Py); 125.85 (5-CH-Py); 126.11 (5-CH-Py); 126.37 (6-CH-Py); 126.71 (4-CH-anil, 5-CH-Py); 128.95 (3,5-CH-anil); 133.10 (4-CH-th); 135.78 (4-C-Py); 135.91 (5-CH-th); 136.06 (4-C-Py); 136.75 (4-C-Py); 137.45 (4-C-Py); 137.86 (2-C-th); 149.74 (1-C-anil); 150.25; 151.39 (5-CH-Py); 151.63 (6-CH-Py); 153.16 (6-CH-Py); 154.58 (2-C-Py); 155.11 (6-CH-Py); 156.39 (2-C-Py); 157.53 (2-C-Py); 157.68 (2-C-Py); 163.57 (COO); 163.71 (COO); 164.95 (CH=N); 206.65 (3-C-th). (Thiophene is denoted as “th”, aniline - as “anil”, bipyridines - as “Py”, respectively). Found: C, 50.24; H, 4.20; N, 6.72; S 2.72. Calc. for $\text{C}_{43}\text{H}_{40}\text{N}_5\text{F}_6\text{O}_8\text{PRuS}$: C, 50.00; H, 3.90; N, 6.78; S, 3.10. High resolution ESI-MS: m/z 888.1637 (calc. for $\text{C}_{43}\text{H}_{40}\text{N}_5\text{O}_8\text{RuS}^+m/z$ 888.1647).

Bis(4,4'-diethoxycarbonyl-2,2'-bipyridine- $\kappa^2\text{N},\text{N}'$)[2-(thio-phen-2-yl- κC^3)pyridine-

κN]ruthenium(II) hexafluorophosphate (6). Red solid. Yield 63%. δH (400 MHz, CDCl_3 , 27 °C): 1.44 (m, 12H, CH₃), 4.43-4.50 (m, 8H, 4CH₂), 6.16 (d, 1H, $^3J_{\text{H,H}} = 4.6\text{Hz}$, 4-H-th), 6.83-6.86 (m, 1H, 4-H-Py1), 7.31 (d, 1H, $^3J_{\text{H,H}} = 6.0\text{Hz}$, 3-H-Py1), 7.35 (d, 1H, $^3J_{\text{H,H}} = 4.6\text{Hz}$, 5-H-th), 7.50-7.52 (m, 1H, 6-H-Py1), 7.56-7.60 (m, 1H, 5-H-Py1), 7.75-7.77 (m, 1H, 6-H-Py), 7.79-7.81 (m, 1H, 6-H-Py), 7.86-7.90 (m, 2H, 5,6-H-Py), 8.05-8.09 (m, 2H, 5,6-H-Py), 8.13 (d, 1H, $^3J_{\text{H,H}} = 6.0\text{Hz}$, 5-H-Py), 8.15 (d, 1H, $^3J_{\text{H,H}} = 6.0\text{Hz}$, 5-H-Py), 8.77 (s, 1H, 3-H-Py), 8.77 (s, 1H, 3-H-Py), 8.84 (s, 1H, 3-H-Py), 8.92 (s, 1H, 3-H-Py). δC (100 MHz, CDCl_3 , 27 °C): 14.11 (CH₃); 14.17 (CH₃); 62.43 (CH₂); 62.54 (CH₂); 62.63 (CH₂); 62.69 (CH₂); 118.49 (6-CH-Py1); 120.84 (4-CH-Py1); 122.02 (3-CH-Py); 122.05 (3-CH-Py); 122.42 (3-CH-Py); 122.53 (3-CH-Py); 125.55 (6-CH-Py); 125.74 (6-CH-Py); 126.18 (5-CH-Py); 129.46 (6-CH-Py); 132.43 (5-CH-Py); 135.26 (2-C-th); 136.1 (4-C-Py); 136.45 (4-C-Py); 137.16 (4-C-Py); 138.15 (4-C-Py); 149.98 (3-CH-Py1); 150.68 (5-CH-Py); 150.80 (6-CH-Py); 151.69 (5-CH-Py); 155.20 (5-CH-Py); 155.42 (2-C-Py); 156.19 (2-C-Py); 157.61 (2-C-Py); 157.69 (2-C-Py); 162.31 (2-C-Py1); 163.55 (COO); 163.66

(COO); 163.74 (COO); 163.85 (COO); 190.08 (3-C-th). (Thiophene is denoted as “th”, pyridine bound with thiophene - as “Py1”, bipyridines - as “Py”, respectively). Found: C, 49.70; H, 4.18; N, 6.99; S, 2.87. Calc. for $C_{41}H_{38}N_5F_6O_8PRuS$: C, 48.91; H, 3.80; N, 6.96; S, 3.18. High resolution ESI-MS: m/z 862.1479 (calc. for $C_{41}H_{38}N_5O_8RuS^+ m/z$ 862.1490). **(4,4'-Dicarboxy-2,2'-bipyridine- κ^2N,N')(4-carboxy-4'-carboxy-late-2,2'-bipyridine- κ^2N,N')[N-((thiophen-2-yl- κC^3)methyliden)aniline- κN]ruthenium(II) (7)**. Synthesized analogously to [26] and purified as follows. The residue was suspended in hot DMF, insoluble fraction was removed by ultracentrifugation (12400 rpm, 1.5 min). The solvent was removed on a rotary evaporator. The residue was dissolved in hot DMF and precipitated with diethyl ether. 18.5 mg (70 %) of dark red solid was obtained. δH (400 MHz, $CD_3OD+NaOD+D_2O$, 27 °C): 6.45 (d, 1H, $^3J_{H,H} = 4.6$ Hz), 6.50 (m, 2H), 6.89-6.90 (m, 3H), 7.63 (d, 1H, $^3J_{H,H} = 6.0$ Hz), 7.66 (br s, 1H), 7.68 (d, 1H, $^3J_{H,H} = 4.6$ Hz), 7.73 (d, 1H, $^3J_{H,H} = 5.5$ Hz), 7.82 (d, 1H, $^3J_{H,H} = 6.0$ Hz), 7.86 (d, 1H, $^3J_{H,H} = 5.5$ Hz), 7.91 (d, 1H, $^3J_{H,H} = 6.0$ Hz), 8.62 (s, 1H), 8.64 (d, 1H, $^3J_{H,H} = 5.5$ Hz), 8.69 (s, 1H), 8.71 (s, 1H), 8.88 (s, 2H). δC (150 MHz, $CD_3OD+NaOD+D_2O$, 27 °C): 123.10; 123.25; 123.37; 123.61; 126.80; 126.89; 127.24; 129.82; 134.64; 136.04; 139.31; 145.04; 145.38; 146.12; 146.73; 149.93; 151.53; 152.82; 153.98; 155.71; 156.62; 158.43; 159.22; 159.45; 166.38; 171.00; 171.15; 171.29; 171.48; 211.14. Found: C, 54.38; H 3.09; N 8.97; S 3.86. Calc. for $C_{35}H_{23}N_5O_8RuS$: C, 54.26; H, 2.99; N, 9.04; S, 4.14. High resolution ESI-MS: m/z 776.0402 (calc. for $C_{35}H_{23}N_5O_8RuS$, $[M+H]^+$, m/z 776.0392).

(4,4'-Dicarboxy-2,2'-bipyridine- κ^2N,N')(4-carboxy-4'-carboxy-late-2,2'-bipyridine- κ^2N,N')[2-(thiophen-2-yl- κC^3)pyridine- κN]ruthenium(II) (8). Synthesized analogously to [26] and purified as follows. The residue was suspended in diethyl ether with addition of a small amount of DCM and MeOH, filtered and dried. 26.4 mg (83%) of dark red solid was obtained. δH (400 MHz, $CD_3OD+NaOD+D_2O$, 27 °C): 6.29 (d, 1H, $^3J_{H,H} = 4.8$ Hz), 6.75-6.79 (m, 1H), 7.37 (m, 1H), 7.42 (d, 1H, $^3J_{H,H} = 4.7$ Hz), 7.56-7.60 (m, 2H), 7.64-7.67 (m, 2H), 7.69-7.71 (dd, 1H, $^3J_{H,H} = 6.0, 1.6$ Hz), 7.83-7.88 (m, 3H), 7.93 (d, 1H, $^3J_{H,H} = 6.0$ Hz), 8.04 (d, 1H, $^3J_{H,H} = 5.9$ Hz), 8.85 (s, 1H), 8.86 (s, 1H), 8.92 (s, 1H), 9.00 (s, 1H). δC (150

MHz, CD₃OD+NaOD+D₂O, 27 °C): 119.08; 120.81; 123.35; 123.49; 123.89; 126.61; 127.67; 129.88; 134.32; 136.81; 137.46; 144.85; 145.23; 146.15; 147.57; 150.30; 151.22; 151.38; 151.83; 155.79; 157.42; 158.52; 159.11; 159.38; 161.62; 164.96; 171.09; 171.13; 171.31; 171.42; 195.93. Found: C, 52.69; H, 3.19; N, 9.29; S, 3.91. Calc. for C₃₃H₂₁N₅O₈RuS: C, 52.94; H, 2.83; N, 9.35; S, 4.28. High resolution ESI-MS: *m/z* 750.0235 (calc. for C₃₃H₂₁N₅O₈RuS, [M+H]⁺ *m/z*: 750.0196).

2.3. Voltammetric study

Electrochemical studies were carried out using an Autolab 100N potentiostat/galvanostat connected to a PC. Voltammograms were recorded using cyclic voltammetry (CV) in DMF solution containing 0.05 M Bu₄NBF₄ as a supporting electrolyte at 20°C in a 10 mL one-compartment electrochemical cell. A stationary Pt disk (d = 3.2 mm) was used as a working electrode; Pt wire served as an auxiliary electrode; a saturated Ag/AgCl/KCl electrode was used as a reference electrode. The potential of the Fc/Fc⁺ redox couple in the experimental conditions was +0.49 V vs. Ag/AgCl/KCl. Oxygen was removed from the cell by purging with dry argon.

2.4. Calculations

The energy levels E(LUMO+m) and E(HOMO-n) of model cations of the complexes **7** and **8** were optimized in DFT/BP calculations using an STO basis set of triple- ζ quality. The equilibrium structures of **7** and **8** were converged with accuracy of 0.01 Å. All calculations were performed using the Amsterdam Density Functional (ADF) program [27,28] version 2013 [29].

2.5. Cell fabrication

Photoanodes were assembled as follows. TCO22-15 fluorinated tin oxide coated 2.9×2.9 cm² glasses (Solaronix®, specific surface resistivity ~15 Ω/sq) were purified by aging in sulfochromic mixture followed by ultrasonication in organic solvents (isopropanol and acetone) and distilled water, and then dried at

50°C in air. The application of Ti-Nanoxide paste (D/SP, Solaronix®), comprising titania powder and α -terpineol as a binding agent, was performed by the standard «doctor blade» technique using a stencil with a 2.0×2.0 cm (~ 90 μm depth) square hole. After the paste application, raw photoanodes were dried at 50°C in air, and then calcined in a muffle furnace at 450°C for 1 hour (heating rate 3 °C·min⁻¹, in air). The thickness of obtained titanium dioxide film was about 15 μm , and it was determined by Alpha-Step D-100 profilometer (KLA-Tencor). Sensitizing of titanium dioxide was performed by soaking of photoanodes in $\sim 5 \cdot 10^{-4}$ M methanol solutions of dyes **7** or **8** for 24 hours. A three-electrode photoelectrochemical cell PECC-2 (Zahner) cell was used for the photoanode potential measurements. The photoanode served as a working electrode and a platinum wire with the surface area of 5 cm² was used as an auxiliary electrode, a silver wire was used as a reference electrode. The voltammetric measurements were performed with IPC Pro MF potentiostat under AM 1.5 global one sun of illumination (100 mW·cm⁻²) provided by a solar simulator (Newport 96000). The illumination power at different distances was determined with Nova apparatus (OPHIR-SPIRICON Inc.). Current-voltage characteristic of DSSCs and photocurrent density at the short-circuit voltage were performed by the two-electrode scheme. The transients of photoanode potential and photocurrent density at the short-circuit voltage were measured under irradiation and in dark condition. The photoanode area was about of 1.0 cm². The illuminated photoanode area was restricted by a mask 0.196 cm². The illumination was performed from the side of TiO₂ photoanode with the adsorbed dye.

3. Results and discussion

3.1. Ligands preparation and cyclometallation

We investigated the already known simplest thiophene-containing compounds that could undergo cycloruthenation. The major advantage of the chosen derivatives **1** and **2** was their ability to be modified easily with substituted anilines in **1** or pyridines in **2**. Compound **1** was synthesized by condensation reac-

tion with aniline [23], and compound **2** was synthesized by sequential thiophene bromination [24] and Kumada coupling [25] with 2-bromopyridine in good yields. It is known that benzene in a η -coordinated ruthenium precursor is easily substituted by anionic ligands [30]. Cyclometallation reaction proceeded smoothly with $[\text{Ru}(\text{C}_6\text{H}_6)\text{Cl}_2]_2$ as a ruthenium source, but the yields of **3** and **4** after purification by column chromatography were quite moderate (Scheme 1).

Scheme 1. Synthesis of cyclometallated thiophenes. Conditions: a) EtOH, aniline, reflux; b) $[\text{Ru}(\text{C}_6\text{H}_6)\text{Cl}_2]_2$; NaOH, KPF_6 ; MeCN, 45°C, 48 h; c) H_2O_2 , HBr, Et_2O ; -17-15°C; d) Mg, Et_2O , reflux; e) 2-bromopyridine; $\text{Ni}(\text{dppp})\text{Cl}_2$; Et_2O , rt.

In general, complexes **3** and **4** are light/oxygen sensitive powders, while they are more stable than 2-phenylpyridine analogue. There are two possible ways to prepare target dyes: the direct reaction with salt of dicarboxylic acid [31] or the sequential formation of ester followed by its hydrolysis [30]. To be able to perform reliable experimental spectroscopic and electrochemical study, the second method was chosen. Esters have much better solubility in organic solvents as compared to free acid complexes, even if the latter are in the sodium salt form.

Scheme 2. Preparation of *ortho*-metallated dyes. Conditions: a) diethyl 2,2'-bipyridine-4,4'-dicarboxylate; EtOH, reflux, 3 h; b) DMF, Et_3N , H_2O , reflux, 15 h.

Ester moieties can be removed by alkaline hydrolysis with a DMF/water/ Et_3N mixture [30] (Scheme 2). The structures of the ester **5** and **6** were proved by NMR (all proton and carbon chemical shifts were assigned by 2D-NMR techniques) and HRMS-ESI. The data obtained for free acids were in agreement with that for the parent esters. Besides elemental analysis the absence of PF_6 counteranion was also confirmed by absence of fluoride signals in ^{19}F -NMR. This fact allowed us to consider compounds **7** and **8** having betain structures [16].

3.2. Crystallography

The structures of complexes **3** and **4** were unambiguously proved by means of X-ray diffraction (Fig. 1).

Figure 1. Structures of $[\text{RuL}(\text{MeCN})_4]^+$ in **3** (a) and $4 \cdot \text{Et}_2\text{O}$ (b) (H atoms at carbon atoms and counterions are omitted for clarity, thermal ellipsoids are given with 30% probability).

These compounds adopted configurations of ligands typical to the previously known ruthenium(II) complexes.[32] Complex **3** crystallizes in the P-1 space group. There were two crystallography independent molecules ($Z = 4$) which had identical coordination geometry, so we described one of them. The ruthenium atom in **3** has distorted octahedral coordination geometry (Fig. 1a). The Ru1 atom coordinates four nitrogen atoms of MeCN molecules (Ru1-N 2.013(4)-2.135(4) Å), nitrogen and σ -bound carbon atoms of chelate anion (Ru1-N1 2.091(4), Ru1-C3 2.022(5) Å). The angle between the planes of C6 and C4S-C=N fragments in L-H is 51.9°. The selected bond lengths (Å) and angles (degrees) in **3** were as follows: S1-C 1.708(6), 1.741(5), C2-C3 1.421(7), C3-C4 1.385(7), N1-C5 1.299(6), N1-C6 1.442(6), N-C (MeCN) 1.138(7)-1.130(7), C1-S1-C4 90.3(3), C2-C3-C4 109.8(5), C5-N1-C6 117.4(4), C3-Ru1-N1 79.4(2), C3-Ru1-N2 90.6(2), C3-Ru1-N3 173.9(2), C3-Ru1-N4 90.7(2), C3-Ru1-N5 94.8(2).

Complex $4 \cdot \text{Et}_2\text{O}$ crystallizes in the P-1 space group. The ruthenium atom in $4 \cdot \text{Et}_2\text{O}$ has distorted octahedral coordination geometry (Fig. 1b). The Ru1 atom in $4 \cdot \text{Et}_2\text{O}$ coordinates four nitrogen atoms of MeCN molecules (Ru-N 2.006(2)-2.048(2) Å), nitrogen and σ -bound carbon atoms of 2-(2-thienyl)pyridine anion (Ru-N 2.060(5) and 2.037(12), Ru-C 2.028(5) and 2.14(3) for two forms of disordered ligand, correspondingly). The selected bond angles (deg) in $4 \cdot \text{Et}_2\text{O}$ are as follows: C1-Ru1-N5 175.0(2), C1-Ru1-N1 78.9(2), N1-Ru1-N4 172.8(2), N2-Ru1-N3 176.99(8), C1A-Ru1-N4 176.9(9), C1A-Ru1-N1A 85.2(9), N1A-Ru1-N5 173.4(8).

3.3. Electrochemical study, absorption spectra and DFT/BP simulations

To get estimation of the HOMO – LUMO levels as well as of the stability of the oxidized and reduced species, electrochemical investigation of compounds **5-8** was performed. Half-wave potential values are listed in Table 1.

Table 1. Half-wave potentials ($E_{1/2}$) and direct/reverse peak separation values (ΔE_p) for **5-8** complexes (0.5mM, Pt, 0.05M Bu_4NBF_4 , DMF, 100 mV/s, vs. Ag/AgCl/ $\text{KCl}_{\text{sat.}}$)

*- the peak potential is indicated; the process is irreversible

As follows from the data given in Table 1, all the compounds are redox active in cathodic and anodic area (Fig.2).

Figure 2. CV curves of 0.5 mM solutions of **5, 6** and **8** (Pt, 0.05M Bu_4NBF_4 , DMF, 100 mV/s, vs. Ag/AgCl ($\text{KCl}_{\text{sat.}}$))

Oxidation of **5-8** is completely reversible (direct/reverse peak separation values are of 60-70 mV at a potential scan rate of 100 mV/s; the corresponding peak current ratios are close to unity), diffusion-controlled and metal-centered for all compounds. The peak potential values are typical for $\text{Ru}^{2+}/\text{Ru}^{3+}$ transformation commonly observed in the potential region of 0.5-0.9 V (vs. Ag/AgCl/KCl) for various pyridine-containing ruthenacycles [16,33–35]. Electrochemical reduction of complexes **5-8** is multi-electron, stepwise and ligand-centered.

More likely, the first two reduction steps correspond to the consecutive reduction of the bipyridine ligands as it has been previously observed for ruthenacycles with the similar coordination environment [16,35]. The third electron might be expected to be transferred to the orbital mainly located on the thiophene-based moiety.

Electrochemical data obtained for compounds **5-6** and **7-8** are given in Table 2 allowing the comparison; the CV curves for complexes **5-6** and **8** are presented in Fig.2. It should be mentioned that for fabrication

of DCCSs, the ruthenium(II) dye is based on mesoporous titania forming Ti-O bond, which is close to the covalent one. Ester compounds **5-6** have covalent C-O-C bond, contrary to **7-8**, which have ionized carboxy group. Thus, both types of compounds should be considered as models since they are not applied directly in the photovoltaic cell. Meanwhile, the peripheral ester or carboxy group can be expected to have not really much influence on the electronic properties of the redox centers. This follows, for instance, from the UV-Vis spectral data which is almost the same for both series (see below). One can expect that the electrochemical potential values for **5-6** and **7-8** compounds also should not differ significantly. The problem is in the presence of protons in compounds **7-8**, which provides an additional cathodic process of hydrogen evolution. The corresponding broad peak is superimposed to pyridine- and thiophene-centered redox processes, which are of interest for characterization of the material and occur in the close potential region resulting in a poor peak resolution. The same situation was also observed in [36]. The other problem is much lower solubility of complexes **7-8** as compared to their **5-6** counterparts. These two factors significantly degraded the accuracy of the measurement of the potential values for the redox-transitions of interest for complexes **7-8**, as compared to **5-6** models, which exhibit three consecutive well distinguished one-electron redox transformations in the cathodic area (see Fig. 2). Thus, the CV curves for complexes **7-8** are much less informative (given in Fig.2. and in SI, Figs. S15 and S16) than that for **5-6**. The electrochemical potential gaps ($E_{\text{Ox}} - E_{\text{Red}}$ values) measured for the compounds under investigation are listed in Table 2. Evidently, the experimental estimation is influenced by the solvation energy, as compared to the corresponding DFT calculated values (see below). However, for the ester derivatives **5** and **6**, in which the ligand-centered reduction is not influenced by the impact of hydrogen evolution impeding the correct estimation of the formal potential values, the coincidence of the electrochemical, spectral and DFT-calculated energy gaps was quite reasonable. The UV-vis absorption spectra of the prepared dyes in methanol solution are presented in Fig. 3 and the corresponding data are summarized in Table 2.

Figure 3. Comparison of experimental UV-vis spectra of compounds (a) **5** (solid) and **6** (dashed) (3.4×10^{-5} M solution in methanol) and (b) **7** (solid) and **8** (dashed) (1×10^{-4} M solution in methanol). For calculated spectra of **7** and **8** and alignment of the energy levels see Figure S17 and footnotes to Table S2. Tangent line on Fig. 3a illustrates an estimation of optical band gap $\Delta E_{\text{optical}}$ (Table 2).

Table 2. UV-vis spectral data and band gap energies. Molar extinction coefficients ($\text{M}^{-1}\text{cm}^{-1}$) for selected maxima wavelengths in visible range are given in parentheses. The $\Delta E_{\text{optical}}$ was obtained by extrapolation of the spectral data (Fig. 3). ΔE_{redox} is the difference between the first oxidation and the first reduction potentials of the complexes. ΔE_{KT} was calculated using the Koopmans' theorem: $\Delta E_{\text{opticalKT}}$ as $E(\text{HOMO}-1) - E(\text{LUMO}+1)$ and $E(\text{HOMO}-2) - E(\text{LUMO}+1)$ gap and $\Delta E_{\text{redoxKT}}$ as $E(\text{HOMO}) - E(\text{LUMO})$ and $E(\text{HOMO}) - E(\text{LUMO}+1)$ gap.

All dyes exhibited absorption bands at two distinct spectrum regions. The intense absorption ($\epsilon > 50000 \text{ M}^{-1}\text{cm}^{-1}$) occurs at around 270-350 nm that can be attributed to the localized $\pi \rightarrow \pi^*$ electron transition located on the ligands. Other broad absorption bands are in the visible region of 370-650 nm with molar absorption coefficient of around $10000 \text{ M}^{-1}\text{cm}^{-1}$ are likely to originate from metal-to-ligand charge transfer (MLCT) transition, which is common for similar Ru(II) compounds.[37–39] As it is well known, MLCT in complexes arise from transfer of electrons from molecular orbitals (MO) with metal-like character to those with ligand-like character, therefore we used data from the spectra by extrapolation of the absorption curve to evaluate the optical band gap of the studied complexes.[40] Having experimental electrochemical and UV-Vis data, it was interesting to compare electrochemical and optical band gap values. there is a relationship described generally by the equation[41]

$$\Delta E_{\text{optical}} = \Delta E_{\text{redox}} + \sum_i a_i$$

where term a_i collects factors not directly derivable from either of these measurable variables. Various factors contributing to this term have been discussed earlier [42]. In particular, this term must include a

correction for the solvation energy differences between different species, and a term to account for the differences in the orbital energies of the species. As it can be seen from comparison of the results of optical and electrochemical measurements (Table 2), this term varies from 0.14 to 0.49 eV for studied complexes. These values are in agreement with literature data [41,42].

The calculated distribution of the density of electronic states (DOS) for models **7** and **8** (considered as monovalent cations with fully protonated carboxylic groups) are given in Fig. 4.

Figure 4. Density of electronic states (DOS) and the energy levels of **7** (a) and **8** (b) sensitizers. The values of $\Delta E_{\text{optical}}^{\text{KT}}$ and $\Delta E_{\text{redox}}^{\text{KT}}$ are given in the Table 2.

The optical and electrochemical gaps $\Delta E_{\text{optical}}$ and ΔE_{redox} were calculated using the Koopmans' theorem as

$$\Delta E_{\text{optical}}^{11} = E(\text{LUMO}+1) - E(\text{HOMO}-1)$$

$$\Delta E_{\text{optical}}^{12} = E(\text{LUMO}+1) - E(\text{HOMO}-2)$$

$$\Delta E_{\text{redox}}^{m,n} = E(\text{LUMO}+m) - E(\text{HOMO}-n)$$

where $n = 0, 1, \dots, 15$; $m = 0, 1, \dots, 14$

The calculated difference between the optical and the electrochemical band gaps is consistent with the experimentally obtained values (Table 2). For the complexes **7** and **8** the ΔE_{redox} values are smaller than those of the compounds **5** and **6** by 0.33 and 0.38 V respectively. These values are consistent with $E(\text{HOMO})-E(\text{LUMO})$ gap change in SCN-containing 2,2'-bipyridine Ru(II) complexes calculated previously by replacement of two of the carboxylic anchoring groups by 4,4'-methyl groups [43]. For compound **7**, the HOMO energy was estimated to be equal -7.49 eV, whereas for **8** it was equal to about -7.47 eV. The HOMO energy difference for these two complexes agrees well with the experimental trend of the oxidation potentials (Table 1). Fig. S1 and Table S1 show that the theoretical results match with the ex-

perimental data well. Our approach allows to partially compensate for the possible inaccuracy of the DFT methods in treatment of the electron correlation effects in the transition metal compounds [44].

For compounds **7** and **8**, the three weak bands located at 563 and 570, 498 and 495, 418 and 409, and two strong bands located at 316 and 313, 305 and 304 nm in the UV-vis range, were observed experimentally. The SCN-containing 2,2'-bipyridine Ru(II) complexes have similar UV-vis spectra [32,41–43]. We focused on the analysis of transitions that generated the peaks of longer wavelength absorptions for both complexes. According to the electronic structure calculations of cations **7** and **8** (Fig. 5), the two most long-wave bands are to be assigned to the $n \rightarrow \pi^*$ absorption of Ru lone pairs delocalized on the 2-thiophene substituent. In the green range of cation **7** and in the yellow of the **8** the HOMO \rightarrow LUMO+6 transition is active (Table S2, Fig. S17).

Figure 5. Electronic transitions of cations defined absorption in visible range of spectrum for **7** (a) and **8** (b) dyes: HOMO \rightarrow LUMO+6 and HOMO-1 and HOMO-2 \rightarrow LUMO+1 being the most long-wave bands in the green (**7**) and the yellow (**8**) ranges, HOMO-1 and HOMO-2 \rightarrow LUMO+6 in the blue range. The band gap HOMO-1 (HOMO-2) – LUMO+1 define $\Delta E_{\text{optical}}$, is consistent with the spectral data. The band gap HOMO – LUMO (LUMO+1) defines ΔE_{redox} , is consistent with the electrochemical data. The forbidden HOMO – LUMO transition is not observed in the optical spectra. The numerical designations show the Ru contribution to corresponding MO(%), elucidating more absorption intensity of dye **8** in yellow and blue ranges.

In the blue range of both cations, HOMO-1 \rightarrow LUMO+1 and HOMO-2 \rightarrow LUMO+1 transitions are active. In the yellow range of spectrum of cation **8**, the absorption of the Ru¹-N⁵ π -bond of the 2-thiophene ligand corresponding to HOMO-3 \rightarrow LUMO+1 transition appears. HOMO \rightarrow LUMO+7 absorption is observed in the blue range of the spectrum. The HOMO \rightarrow LUMO+6 transition energy of cation **7** coincides with the maximum of the most long-wave band. In cation **8**, this transition is hypsochromically shifted by the val-

ue of 65 nm. The similar shift of 68 nm was also found for the HOMO→LUMO+7 transition. The absence of the same shift for the HOMO→LUMO+6 of cation **7** can be explained by the absence of the solvent effect because of equivalence of the bond conjugation chain length of atoms, on which these MOs are delocalized (HOMO: Ru¹-N⁵-C²⁴-C^{1a}-C²²-S²¹ and LUMO+6: Ru¹-N⁵-C²⁵-C^{1a}-C²²-S²¹, Fig. 5, Fig. S17) and the same Mulliken atomic charges values on the C²²-S²¹ atoms (Table S3), suitable for the formation of the complex with solvent CH₃OH [44]. Thus, the influences of the solvent on HOMO and LUMO+6 energies of cation **7** are equal. However, in cation **8**, the bond conjugation chain of atoms on which the LUMO+6 is delocalized is longer than that for the HOMO. Therefore, the solvent effect results into the decrease of the HOMO-LUMO+6(7) gap and bathochromic shift of this transition. The stabilization of the ground state of the transition metal compounds, as a conjugation effect between the metallaallene fragment and the co-planar phenyl ring [48], and abrupt change of dye properties by the decrease of the bond conjugation chain length were reported previously [49–51]. In cations **7** and **8**, the difference between experimental and calculated values of wavelengths of the blue range transitions of 41 (44) and 67 (82) nm may be explained in the same way. The values of these transitions depend on the lone pair localization on Ru, as well as on the Mulliken atomic charges distributions (Fig. 5 and Table S3). The violet range band (Fig.S16, Table S1) is due to

- (i) Absorption of: the 4,4'-dicarboxy-2,2'-bipyridine ligands with electron transitions from the HOMO-12 (**7**) or HOMO-11 (**8**) to the LUMO and from the HOMO-13 (**7**) or HOMO-10 (**8**) to the LUMO+1;
- (ii) Absorption of the Ru¹-N⁵ π-bond of 2-thiophene ligand with electron transition between the HOMO-3 and LUMO+6;
- (iii) In cation **7**, the HOMO-12→LUMO+1, HOMO-13→LUMO transitions are active, too. In cation **8** there is also the Ru lone pairs' absorption corresponding to the transitions from the HOMO or HOMO-2 to LUMO+7. The absence of the similar LUMO of appropriate energy in cation **7** explains the higher in-

tensity of the violet band of the **8** dye. Strong absorption in near UV is mostly due to $\pi \rightarrow \pi^*$ transitions of the 4,4'-dicarboxy-2,2'-bipyridine ligands. All electronic transitions in the visible and NIR ranges are forbidden by the well-known selection rules; therefore, the intensity of absorption is weak. Fig. 5 shows electronic transitions that define the long-wave absorption bands. These $n \rightarrow \pi^*$ transitions are almost forbidden and have low intensity. In cation **8**, comparing with **7**, the contribution of Ru in HOMO and HOMO-2 is smaller, and it is larger in HOMO-1. The HOMO-2 (**8**) is more delocalized and HOMO-1 (**8**) is less delocalized on the anionic ligand. The symmetry change from n to π increases probability of transition and its intensity. This determines higher intensity and a small bathochromic shift in the green range, and a hypsochromic shift of bands in the blue range of UV-vis spectrum of the **8** dye in comparison to dye **7**.

3.4. Photovoltaic performance

After injecting the electron into the conduction band of TiO_2 , regeneration of the dye is an important process within DSSC. To date, iodide/triiodide has been the most efficient redox couple used for high-performance DSSCs. The physical diffusion of iodide/triiodide in the electrolyte is often a limiting process. We used the method of photopotential and photocurrent transients to study the dye regeneration process. The results are presented in Fig. 6.

Figure 6. (a) Photoanode potential versus time for the DSSC with the anodes stained with **7** (dash line) and **8** (solid line) dyes in dark condition and under illumination with power of $100 \text{ mW} \cdot \text{cm}^{-2}$. (b) Photocurrent density transient at the short-circuit voltage for the DSSCs with the anodes stained with **7** (dash line) and **8** (solid line) dyes in dark condition and under illumination with power of $100 \text{ mW} \cdot \text{cm}^{-2}$.

The potential rapidly shifted towards negative values upon illumination, which indicates that there is high-rate accumulation of injected electrons in the TiO_2 conduction band. This suggests that the excited level of the dyes lay higher in energy than the bottom of the conduction band, and that there is a sponta-

neous process of charge transfer from the excited state of dye into the band. It is to be noted that there is no degradation of photopotential over the time. Fig. 6 shows the photocurrent response to the light on-off sequence. One can see that the DSSCs with **7** and **8** dyes exhibit the current remaining constantly. These results indicate that in the case of the iodide/triiodide system there is no diffusion limitation on the regeneration of the dyes, according to Zakeeruddin [52]. The photovoltaic performance is shown in Fig. 7 and Table 3.

Figure 7. Current-voltage characteristic of DSSCs with the photoanodes made using the sensitizers **7** (dash line) and **8** (solid line) upon illumination ($100 \text{ mW}\cdot\text{cm}^{-2}$).

Table 3. DSSC performance data.

*Solaronix® N535 – bis(4,4'-dicarboxy-2,2'-bipyridine- $\kappa^2\text{N,N}'$)ruthenium(II) cis-dithiocyanate

It was found that DSSCs have similar characteristics. However, a comparison of I-V characteristics shows that dye **7** photocurrent density and open circuit voltage exceed those of the **8** dye. For comparison, the corresponding parameters are also shown for the standard N535 dye and for the known cycloruthenated thiophenes (see Table 3). From the photovoltaic data it is apparent that the new synthetically facile ruthenium(II) complexes are promising dyes for DSSCs overall conversion efficiency improvement. The study of various **7** and **8** derivatives will be continued to find out the optimal configuration of the substituents for better DSSCs performance.

Further improvement in the efficiency DSSC with the **7** and **8** sensitizers is possible by choosing of doping of titania with rare-earth metal complexes [53], tuning of electrolyte composition [4] and choosing optimal configuration of substituents. The work directed towards this goal is in progress.

4. Conclusions

Two bis-heteroleptic ruthenium(II) dyes containing different types of the simplest cyclometallated thiophene moieties were synthesized and characterized by NMR, UV-vis spectroscopy and cyclic voltammetry. *Ortho*-metallation of thiophenes was proved by means of single crystal X-ray data. To get an insight of the influence of the substituents in the thiophene ligand on the electronic structure of the complexes, DFT calculations of the energy and localization of their molecular orbitals were performed. Theoretical and experimental estimations of the energy band gaps are in good agreement. Synthesized complexes are of interest for the fabrication of dye-sensitized solar cells. The estimation of an overall conversion efficiency range of new sensitizers gave values from 4.1 to 5.3% under standard AM 1.5 sunlight, which are only slightly lower than that of the standard ruthenium N535 dye exhibiting 6.1% PCE but higher than of other known cycloruthenated thiophenes.

Acknowledgements

The study was supported by RFBR (project 13-03-12415), RSF (project 14-23-00176), and by Tomsk State University Competitiveness Improvement Program. We thank Prof. P. Dyachkov and Dr. D. Krut'ko for fruitful and useful discussions.

Appendix A. Supplementary data

The following is the supplementary data related to this article:

References

- [1] IEA-PVTS. PVPS Report Snapshot of Global PV 1992-2013. 2014.
- [2] Green MA, Emery K, Hishikawa Y, Warta W. Solar cell efficiency tables (version 35). *Prog Photovoltaics Res Appl* 2010;18:144–50. doi:10.1002/pip.974.
- [3] Optimal Materials and Deposition Technique Lead to Cost-Effective Solar Cell with Best-Ever Conversion Efficiency. Report of the National Renewable Energy Laboratory, 2012.

- [4] Mathew S, Yella A, Gao P, Humphry-Baker R, Curchod BFE, Ashari-Astani N, et al. Dye-sensitized solar cells with 13% efficiency achieved through the molecular engineering of porphyrin sensitizers. *Nat Chem* 2014;6:242–7. doi:10.1038/nchem.1861.
- [5] Yella A, Lee H-W, Tsao HN, Yi C, Chandiran AK, Nazeeruddin MK, et al. Porphyrin-sensitized solar cells with cobalt (II/III)-based redox electrolyte exceed 12 percent efficiency. *Science* (80-) 2011;334:629–34. doi:10.1126/science.1209688.
- [6] Park N-G. Perovskite solar cells: an emerging photovoltaic technology. *Mater Today* 2015;18:65–72.
- [7] Nazeeruddin MK, Kay A, Rodicio I, Humphry-Baker R, Mueller E, Liska P, et al. Conversion of light to electricity by cis-X₂bis(2,2'-bipyridyl-4,4'-dicarboxylate)ruthenium(II) charge-transfer sensitizers (X = Cl⁻, Br⁻, I⁻, CN⁻, and SCN⁻) on nanocrystalline titanium dioxide electrodes. *J Am Chem Soc* 1993;115:6382–90. doi:10.1021/ja00067a063.
- [8] Bomben PG, Robson KCD, Koivisto BD, Berlinguette CP. Cyclometalated ruthenium chromophores for the dye-sensitized solar cell. *Coord Chem Rev* 2012;256:1438–50. doi:10.1016/j.ccr.2012.02.005.
- [9] Yin J-F, Velayudham M, Bhattacharya D, Lin H-C, Lu K-L. Structure optimization of ruthenium photosensitizers for efficient dye-sensitized solar cells – A goal toward a “bright” future. *Coord Chem Rev* 2012;256:3008–35. doi:10.1016/j.ccr.2012.06.022.
- [10] Chen C-Y, Wang M, Li J-Y, Pootrakulchote N, Alibabaei L, Ngoc-le C-H, et al. Highly efficient light-harvesting ruthenium sensitizer for thin-film dye-sensitized solar cells. *ACS Nano* 2009;3:3103–9. doi:10.1021/nn900756s.
- [11] Zakeeruddin SM, Nazeeruddin MK, Humphry-Baker R, Grätzel M, Shklover V. Stepwise Assembly of Tris-Heteroleptic Polypyridyl Complexes of Ruthenium(II). *Inorg Chem* 1998;37:5251–9. doi:10.1021/ic980357s.

- [12] Bessho T, Yoneda E, Yum J-H, Guglielmi M, Tavernelli I, Imai H, et al. New paradigm in molecular engineering of sensitizers for solar cell applications. *J Am Chem Soc* 2009;131:5930–4. doi:10.1021/ja9002684.
- [13] Pogozhev D V., Bezdek MJ, Schauer PA, Berlinguette CP. Ruthenium (II) Complexes Bearing a Naphthalimide Fragment: A Modular Dye Platform for the Dye-Sensitized Solar Cell. *Inorg Chem* 2013;52:3001–6.
- [14] Brown DG, Schauer PA, Borau-Garcia J, Fancy BR, Berlinguette CP. Stabilization of ruthenium sensitizers to TiO₂ surfaces through cooperative anchoring groups. *J Am Chem Soc* 2013;135:1692–5. doi:10.1021/ja310965h.
- [15] Schulze B, Escudero D, Friebe C, Siebert R, Görls H, Sinn S, et al. Ruthenium(II) photosensitizers of tridentate click-derived cyclometalating ligands: a joint experimental and computational study. *Chem - A Eur J* 2012;18:4010–25. doi:10.1002/chem.201103451.
- [16] Bomben PG, Koivisto BD, Berlinguette CP. Cyclometalated Ru complexes of type [Ru(II)(N--N)(2)(C--N)](z): physicochemical response to substituents installed on the anionic ligand. *Inorg Chem* 2010;49:4960–4671. doi:10.1021/ic100063c.
- [17] Cuesta L, Urriolabeitia EP. Cyclometallation of Heterocycles: A Reliable Strategy for Selective Functionalization. *Comments Inorg Chem* 2012;33:55–85. doi:10.1080/02603594.2012.700971.
- [18] Li X-H, Shi Z, Wang L, Cheng X, Li C, Zhang A. Chromogenic mercury ions recognition of a new ruthenium(II) complex with cyclometalated 2-(2-thienyl)pyridine in CH₃CN-aqueous system. *Inorg Chem Commun* 2013;29:175–8. doi:10.1016/j.inoche.2012.12.004.
- [19] Li C-Y, Su C, Wang H-H, Kumaresan P, Hsu C-H, Lee I-T, et al. Design and development of cyclometalated ruthenium complexes containing thiophenyl-pyridine ligand for dye-sensitized solar cells. *Dye Pigment* 2014;100:57–65. doi:10.1016/j.dyepig.2013.07.014.
- [20] Vriamont N, Govaerts B, Grenouilles P, de Bellefon C, Riant OXX. Design of a genetic algorithm

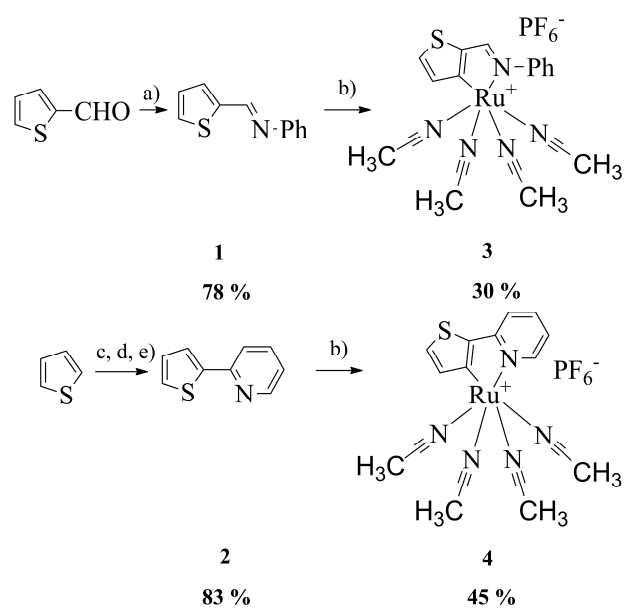
- for the simulated evolution of a library of asymmetric transfer hydrogenation catalysts. *Chem - A Eur J* 2009;15:6267–78.
- [21] Gillaizeau-Gauthier I, Odobel F, Alebbi M, Argazzi R, Costa E, Bignozzi CA, et al. Phosphonate-Based Bipyridine Dyes for Stable Photovoltaic Devices. *Inorg Chem* 2001;40:6073–9. doi:10.1021/ic010192e.
- [22] Tsedilin AM, Fakhrutdinov AN, Eremin DB, Zalesskiy SS, Chizhov AO, Kolotyrykina NG, et al. How sensitive and accurate are routine NMR and MS measurements? *Mendeleev Commun* 2015;25:454–6. doi:10.1016/j.mencom.2015.11.019.
- [23] Wang D-L, Hwang W, Liang L, Wang L-I, Lee L, Chiang MY. Reaction of a Thienyl Schiff Base with Diiron Nonacarbonyl: Characterization and Structures of $[\mu\text{-N}((2,3\text{-}\eta^1\text{-}2\text{-thienyl)methyl)\text{-}\eta^1\text{-}1\text{-N}(\text{anilino})\text{-}hexacarbonyl]diiron$ and $[\mu\text{-N}((2\text{-thienyl)methyl)((2,3\text{-}\eta^1\text{-}2\text{-thienyl}))\text{-}2\text{-thienyl}]$. *Organometallics* 1997;16:3109–13. doi:10.1021/om961092x.
- [24] Keegstra MA, Brandsma L. Convenient high-yield procedures for 2-bromothiophene and 2,5-dibromothiophene. *Synthesis (Stuttg)* 1988:890–1.
- [25] Novak I, Ng S, Mok C, Huang H, Fang J, Wang KK. New organic polymer precursors: synthesis and electronic structure of thienylpyridines and thienylethynylpyridines. *J Chem Soc Perkin Trans 2* 1994:1771. doi:10.1039/p29940001771.
- [26] Bomben PG, Gordon TJ, Schott E, Berlinguette CP. A trisheteroleptic cyclometalated Ru(II) sensitizer that enables high power output in a dye-sensitized solar cell. *Angew Chemie - Int Ed* 2011;50:10682–5. doi:10.1002/anie.201104275.
- [27] Guerra CF, Snijders JG, te Velde G, Baerends EJ. Towards an order-N DFT method. *Theor Chem Acc* 1998;99:391–403. doi:10.1007/s002140050353.
- [28] te Velde G, Bickelhaupt FM, Baerends EJ, Guerra CF, van Gisbergen SJA, Snijders JG, et al.

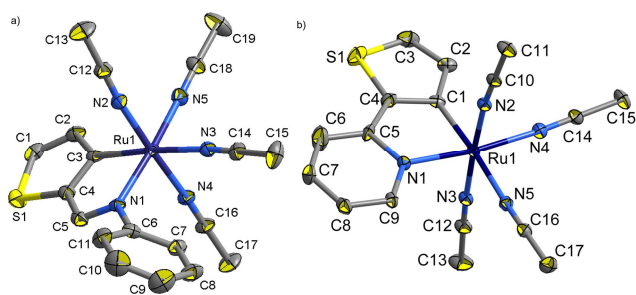
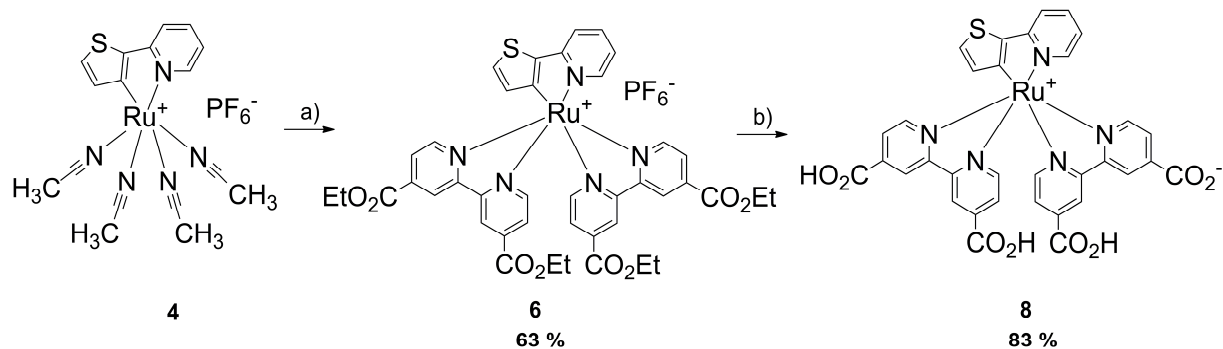
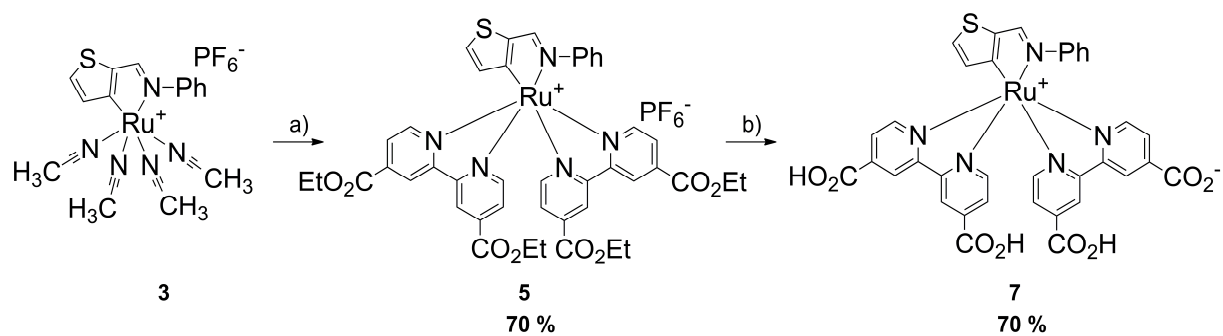
Chemistry with ADF. *J Comput Chem* 2001;22:931–67. doi:10.1002/jcc.1056.

- [29] ADF® molecular modeling suite 2013.
- [30] Bomben PG, Thériault KD, Berlinguette CP. Strategies for Optimizing the Performance of Cyclometalated Ruthenium Sensitizers for Dye-Sensitized Solar Cells. *Eur J Inorg Chem* 2011;2011:1806–14. doi:10.1002/ejic.201001345.
- [31] Bomben PG, Robson KCD, Sedach P, Berlinguette CP. On the viability of cyclometalated Ru(II) complexes for light-harvesting applications. *Inorg Chem* 2009;48:9631–43. doi:10.1021/ic900653q.
- [32] Cuesta L, Maluenda I, Soler T, Navarro R, Urriolabeitia EP. Novel thiophene-based cycloruthenated compounds: synthesis, characterization, and reactivity. *Inorg Chem* 2011;50:37–45. doi:10.1021/ic101946n.
- [33] Yap JSL, Li B Bin, Wong J, Li Y, Pullarkat SA, Leung P-H. Development of a novel chiral palladacycle and its application in asymmetric hydrophosphination reaction. *Dalt Trans* 2014;43:5777. doi:10.1039/c4dt00062e.
- [34] Djukic J-P, Sortais J-B, Barloy L, Pfeffer M. Cycloruthenated Compounds - Synthesis and Applications. *Eur J Inorg Chem* 2009;2009:817–53. doi:10.1002/ejic.200801016.
- [35] Robson KCD, Bomben PG, Berlinguette CP. Cycloruthenated sensitizers: improving the dye-sensitized solar cell with classical inorganic chemistry principles. *Dalt Trans* 2012;41:7814. doi:10.1039/c2dt30825h.
- [36] Dragonetti C, Valore A, Colombo A, Magni M, Mussini P, Roberto D, et al. Ruthenium oxyquinolate complexes for dye-sensitized solar cells. *Inorganica Chim Acta* 2013;405:98–104. doi:10.1016/j.ica.2013.05.006.
- [37] Tobe ML, Burgess J. *Inorganic Reaction Mechanisms*. Addison Wesley Longman Ltd.; 1999.
- [38] Ruile S, Kohle O, Péchy P, Grätzel M. Novel sensitizers for photovoltaic cells. *Structural*

- variations of Ru(II) complexes containing 2,6-bis(1-methylbenzimidazol-2-yl)pyridine. *Inorganica Chim Acta* 1997;261:129–40. doi:10.1016/S0020-1693(97)05457-1.
- [39] Zakeeruddin SM, Nazeeruddin MK, Humphry-Baker R, Grätzel M. Synthesis and photophysical properties of trans-dithiocyanato bis(4,4'-dicarboxylic acid-2,2'-bipyridine) ruthenium(II) charge transfer sensitizer. *Inorganica Chim Acta* 1999;296:250–3. doi:10.1016/S0020-1693(99)00359-X.
- [40] Tarr DA, Miessler GL. *Inorganic chemistry*. 2nd ed. Englewood Cliffs, N.J: Prentice Hall; 1991.
- [41] Vlcek A, Dodsworth ES, Pietro WJ, Lever BP. Excited State Redox Potentials of Ruthenium Diimine Complexes; Correlations with Ground State Redox Potentials and Ligand Parameters. *Inorg Chem* 1995;34:1906–13. doi:10.1021/ic00111a043.
- [42] Dodsworth ES, Lever ABP. Correlation of electronic charge transfer transitions and electrochemical potentials. *Chem Phys Lett* 1984;112:567–70. doi:10.1016/0009-2614(84)85780-2.
- [43] Azpiroz JM, De Angelis F. DFT/TDDFT study of the adsorption of N3 and N719 dyes on ZnO(1010) surfaces. *J Phys Chem A* 2014;118:5885–93. doi:10.1021/jp501058x.
- [44] Shorokhov D, Park ST, Zewail AH. Ultrafast electron diffraction: Dynamical structures on complex energy landscapes. *ChemPhysChem* 2005;6:2228–50. doi:10.1002/cphc.200500330.
- [45] Baryshnikov G V., Minaev BF, Minaeva VA. Quantum-chemical study of effect of conjugation on structure and spectral properties of C105 sensitizing dye. *Opt Spectrosc* 2011;110:393–400. doi:10.1134/S0030400X10061025.
- [46] Nazeeruddin MK, De Angelis F, Fantacci S, Selloni A, Viscardi G, Liska P, et al. Combined experimental and DFT-TDDFT computational study of photoelectrochemical cell ruthenium sensitizers. *J Am Chem Soc* 2005;127:16835–47. doi:10.1021/ja0524671.
- [47] Barolo C, Nazeeruddin MK, Fantacci S, Di Censo D, Comte P, Liska P, et al. Synthesis, characterization, and DFT-TDDFT computational study of a ruthenium complex containing a

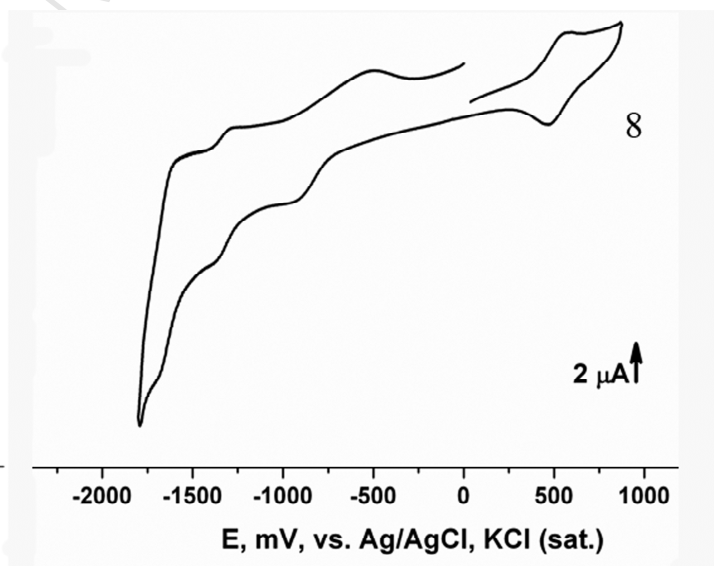
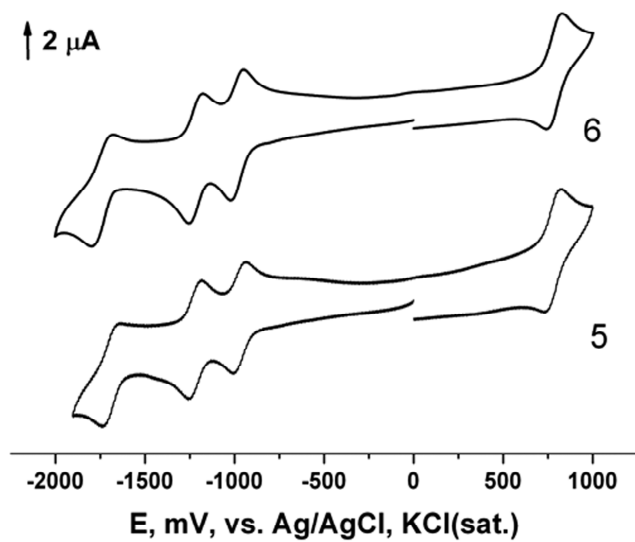
- functionalized tetradentate ligand. *Inorg Chem* 2006;45:4642–53. doi:10.1021/ic051970w.
- [48] Ivanova-Shor EA, Nasluzov VA, Shor AM, Antonova AB, Rösch N. Vinylidene carbonylation at a manganese-iron complex: A density functional study of mechanism. *J Organomet Chem* 2011;696:3445–53. doi:10.1016/j.jorganchem.2011.06.051.
- [49] Apostolova ES, Eltsov A V. Quantum chemical study of complex of dianion forms of fluorescein and its thioanalog with nucleophile. *Zhurnal Obs Khimii* 1991;61:1236–40.
- [50] Apostolova ES, Eltsov A V. Quantum chemical computation of the effect of the nature of heteroatom and phenyl substituent on electron characteristics of xanthene dye dianion forms. *Zhurnal Obs Khimii* 1990;60:2606–2014.
- [51] Apostolova ES, Smirnova NP, Eltsov A V. Influence of nucleophilic substituents and heteroatom nature on electronic structure and properties of thiophen analogs of fluorescein. *Zhurnal Obs Khimii* 1992;62:2750–6.
- [52] Zakeeruddin SM, Grätzel M. Solvent-free ionic liquid electrolytes for mesoscopic dye-sensitized solar cells. *Adv Funct Mater* 2009;19:2187–202. doi:10.1002/adfm.200900390.
- [53] Wang X, Yang Y-L, Wang P, Li L, Fan R-Q, Cao W-W, et al. High efficiency co-sensitized solar cell based on luminescent lanthanide complexes with pyridine-2,6-dicarboxylic acid ligands. *Dalt Trans* 2012;41:10619–25. doi:10.1039/c2dt30430a.

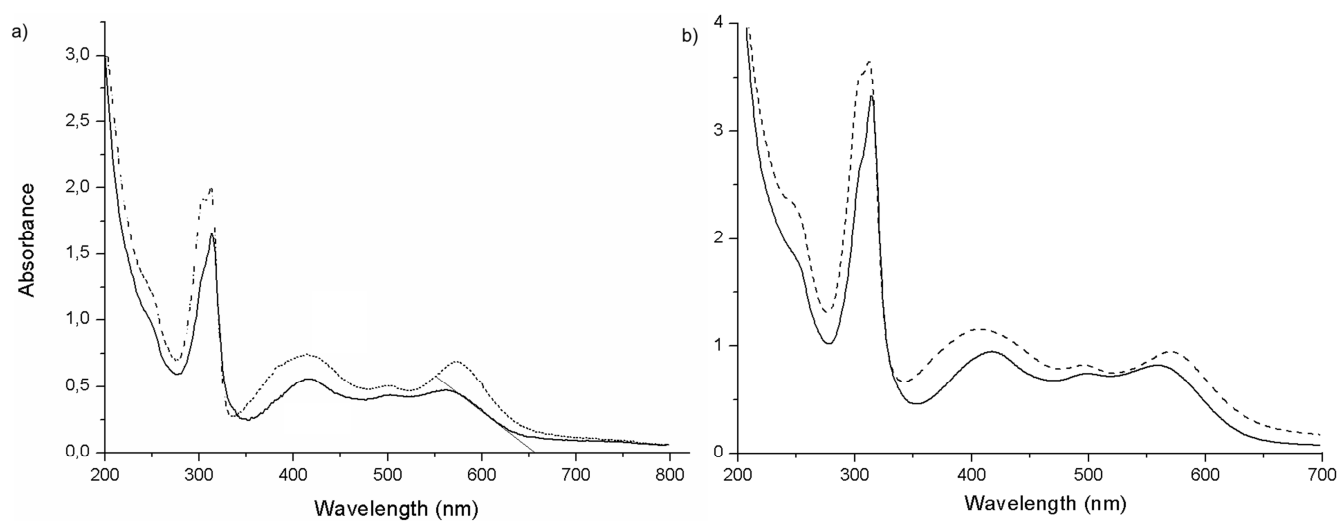




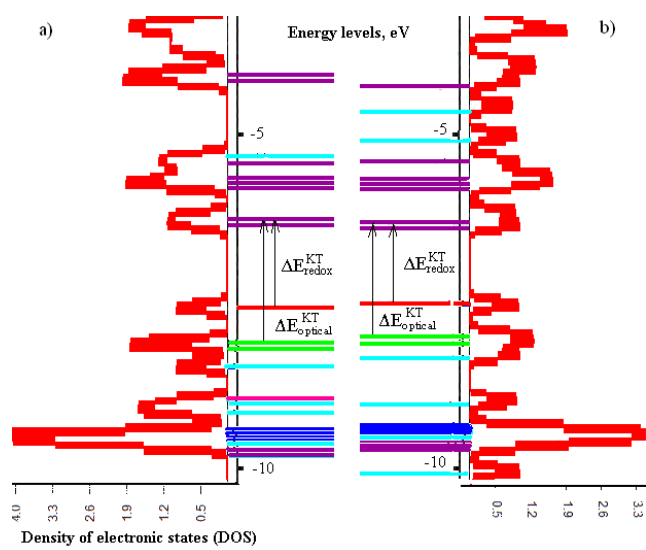
Complex	$-E_{1/2\text{Red}}, \text{V}$	$\Delta E_p, \text{V}$	$E_{1/2\text{Ox}}, \text{V}$	$\Delta E_p, \text{V}$
5	0.99	0.06	0.80	0.06
	1.22	0.07		
	1.75	0.09		

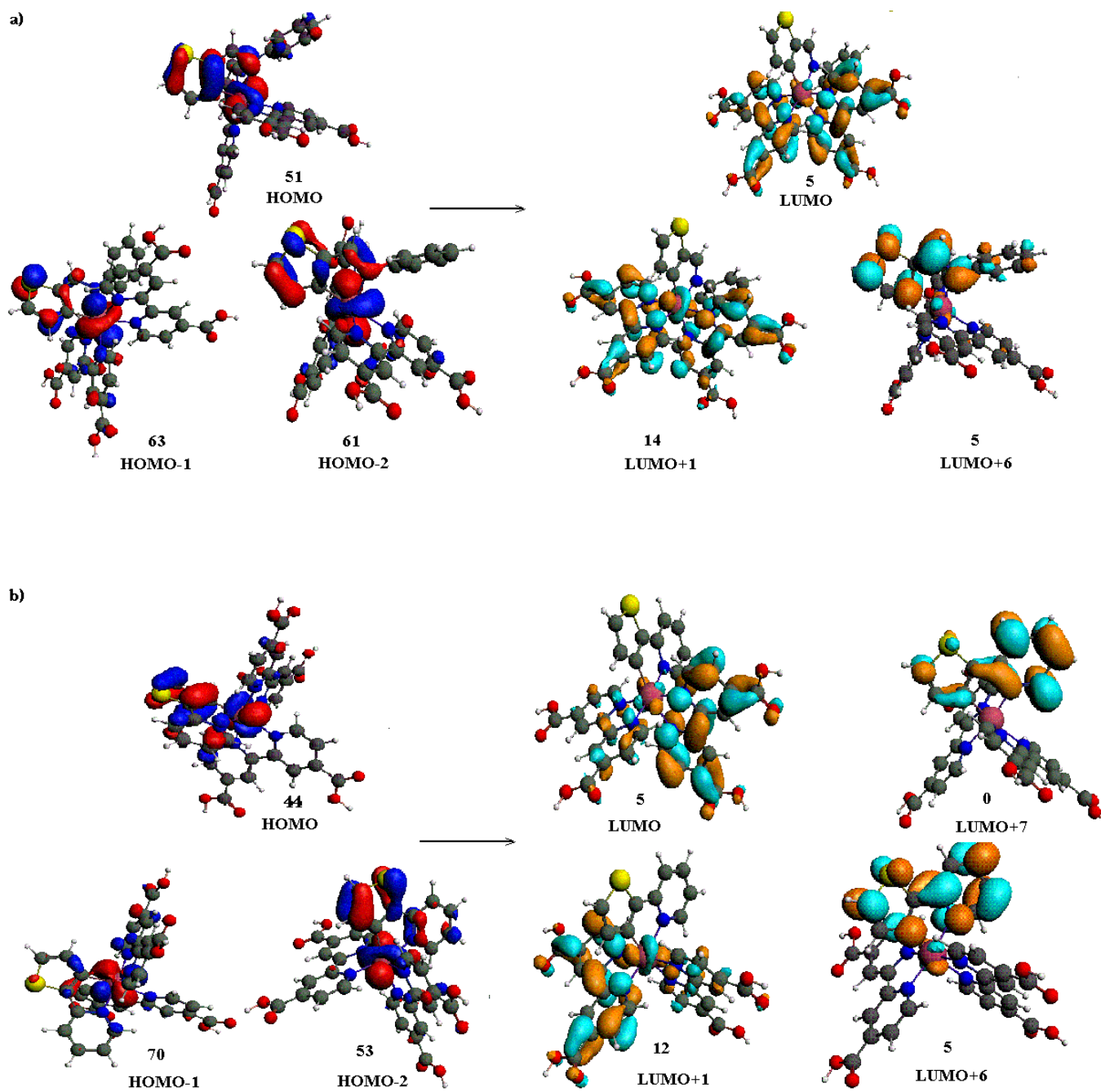
6	0.97	0.06		
	1.23	0.07	0.79	0.06
	1.71	0.08		
7	0.91*		0.59	0.07
	1.65 (2e)	0.07		
8	0.90*			
	1.33	0.07	0.52	0.07
	1.65	0.09		

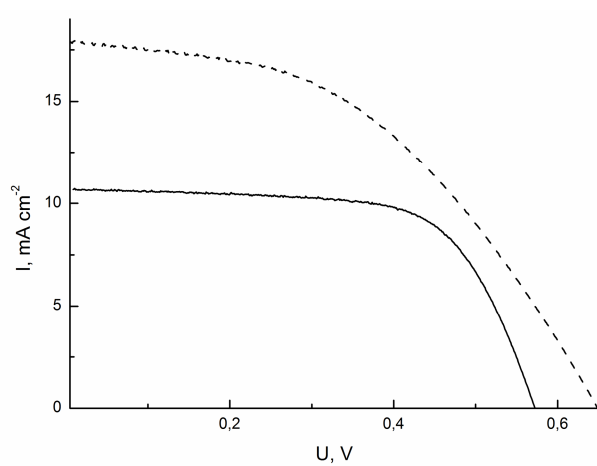
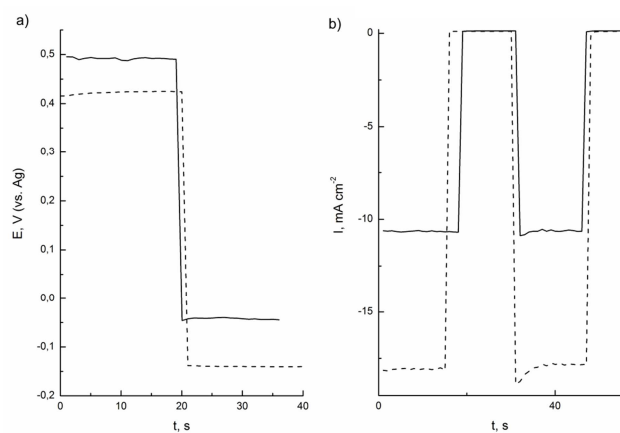




Complex	Peaks, nm	Band gap energy, eV			
		$\Delta E_{\text{optical}}$, eV	ΔE_{redox} , V	$\Delta E_{\text{redoxKT}}$, eV	$\Delta E_{\text{opticalKT}}$, eV
5	415 (16600), 503 (12800), 562 (14000)	1.93	1.79	-	-
6	418 (22000), 498 (14800), 573 (20500)	1.92	1.76	-	-
7	418 (9500), 498 (7600), 563 (8200)	1.94	1.46	1.21 1.34	1.84 1.86
8	409 (11500), 495 (8400), 570 (9600)	1.87	1.38	1.16 1.34	1.78 1.89







Complex	J_{sc} , mA·cm ⁻²	V_{oc} , V	Fill factor, %	Efficiency, %
7	18.0	0.65	46	5.3
8	10.7	0.58	65	4.1
Solaronix® N535*	16.5	0.71	53	6.1

NC102 [19]	8.15	0.63	71	3.64
NC103 [19]	9.45	0.63	71	4.22

ACCEPTED MANUSCRIPT

Highlights

- Two cycloruthenated thiophene dyes of different types were synthesized.
- Cycloruthenation was confirmed with single crystal X-ray experiment.
- UV spectroscopy and cyclic voltammetry measurements compared with DFT calculations.
- Power conversion efficiencies of sensitizers are in range from 4.1 to 5.3%.